

ANALYSIS OF VIEW ALIASING FOR THE GENERALIZED RADON TRANSFORM IN \mathbb{R}^2

ALEXANDER KATSEVICH¹

ABSTRACT. In this paper we consider the generalized Radon transform \mathcal{R} in the plane. Let f be a piecewise smooth function, which has a jump across a smooth, convex curve \mathcal{S} . We obtain a precise, quantitative formula describing view aliasing artifacts when f is reconstructed from the data $\mathcal{R}f$ discretized in the view direction. The formula is asymptotic, it is established in the limit as the sampling rate $\epsilon \rightarrow 0$. The proposed approach does not require that f be band-limited. Numerical experiments with the classical Radon transform and generalized Radon transform (which integrates over circles) demonstrate the accuracy of the formula.

1. INTRODUCTION

Resolution of image reconstruction from discrete data is one of the fundamental questions in imaging. The most direct approach to estimating resolution utilizes the notions of the point spread function (PSF) and modulation transfer function (MTF) [1, Sections 12.2, 12.3]. This and other similar approaches allow rigorous theoretical analysis of only the simplest settings, such as inversion of the classical Radon transform. For the most part, resolution of reconstruction in more difficult settings (e.g., inversion of the cone beam transform) is analyzed by heuristic arguments, numerically, or via measurements [2–4].

Sampling theory provides another approach to investigating resolution [5–14]. Consider, for example, the classical Radon transform in \mathbb{R}^2

$$(1.1) \quad \hat{f}(\alpha, p) = \int_{\mathbb{R}^2} f(x) \delta(\vec{\alpha} \cdot x - p) dx, \quad \vec{\alpha} = (\cos \alpha, \sin \alpha).$$

The corresponding discrete data are

$$(1.2) \quad \hat{f}(\alpha_k, p_j), \quad \alpha_k = \bar{\alpha} + k\Delta\alpha, \quad p_j = \bar{p} + j\Delta p, \quad \alpha_k \in [0, 2\pi), \quad j \in \mathbb{Z},$$

for some fixed $\bar{\alpha}$, \bar{p} and $\Delta\alpha$, Δp . Assume that f is essentially band-limited (in the classical sense). This means that, with high accuracy, its Fourier transform $\hat{f}(\xi)$ is supported in some ball $|\xi| \leq B$. The sampling theory predicts the rates $\Delta\alpha$, Δp with which $\hat{f}(\alpha, p)$ should be sampled, so that reconstruction of f from discrete data does not contain aliasing artifacts. Since the essential band-limit B is related to the size of the smallest detail in f , a typical prescription of the theory can be loosely formulated as follows: given the size of the smallest detail in f , the minimal sampling rates to avoid aliasing are $\Delta\alpha$, Δp . Alternatively, the theory determines the size of the smallest detail in f that can be resolved given the rates $\Delta\alpha$, Δp .

A microlocal approach to sampling was developed recently [15–17]. In this approach f is assumed to be band-limited in the semiclassical sense (i.e., the semiclassical wavefront set $\text{WF}_h(f)$ is compact). The goal is to accurately recover the semiclassical singularities of f and avoid aliasing. If the sampling requirement is violated, the theory predicts the location and frequency of the aliasing artifacts.

¹This work was supported in part by NSF grant DMS-1906361. Department of Mathematics, University of Central Florida, Orlando, FL 32816 (Alexander.Katsevich@ucf.edu).

At a high level, the classical and semiclassical sampling theories are similar in two aspects. First, both assume that f is band-limited. Second, in both of them the size of the smallest detail in f determines the sampling rate of \hat{f} , and the sampling rate determines the smallest detail in f that can be resolved.

This implies that the practical use of the sampling theory to precisely quantify the resolution of reconstruction is, in many cases, not fully justified. Indeed, the vast majority of objects being scanned are nonsmooth and have sharp edges, so, strictly speaking, they are not band-limited. Therefore, specifying an approximate band-limit for the function f that describes such an object is fairly arbitrary. Second, the notion of resolving a detail in f is somewhat arbitrary too. There is no threshold such that the given feature is resolved if the sampling rate is smaller than the threshold, and the feature is not resolved if the sampling rate is greater than the threshold. There is always a smooth transition between resolving a feature and not resolving a feature. Finally, if a feature in f is resolved according to the sampling theory, the theory does not specify what the reconstruction of the feature looks like. For these three reasons, in practice, the notions of a band-limit (both classical and semiclassical) and the size of the smallest detail provide a ballpark estimate of resolution rather than its precise value.

In [18–22], the author developed an analysis of resolution (we call it Local Resolution Analysis, or LRA), which addresses the question of resolution head on. The main results in these papers are simple expressions describing the reconstruction from discrete data in a neighborhood of the singularities of f in a variety of settings. We call these expressions the Discrete Transition Behavior (DTB). The DTB provides the most direct, fully quantitative link between the sampling rate and resolution. In these papers such a link is established for a wide range of integral transforms, conormal distributions f , and reconstruction operators. In [23, 24] LRA was generalized to objects with rough boundaries in \mathbb{R}^2 .

Suppose $\Delta p = \epsilon$ and $\Delta \alpha = \kappa \epsilon$, where $\kappa > 0$ is fixed. The DTB is an accurate approximation of the reconstruction in an ϵ -neighborhood of the singular support of f in the limit as $\epsilon \rightarrow 0$. Therefore, the DTB provides much more than a single measure of resolution (e.g., the size of the smallest detail that can be resolved). Given the DTB function, the user may decide in a fully quantitative way what sampling rate is required to achieve the user-defined reconstruction quality. The notion of quality may include resolution (which can be described in any desired way) and/or any other requirement the user desires. Thus, the LRA answers precisely the question of the required sampling rate to guarantee the required resolution (understood broadly). No assumption that f be band-limited (either classically or semiclassically) is required.

The only item missing from the LRA until now was an analysis of aliasing. In practice f is almost never band-limited, so aliasing artifacts arise regardless of the sampling rate. Some earlier results on the analysis of aliasing artifacts (more precisely, view aliasing artifacts) are in [25] and [1, Section 12.3.2]. They include an approximate formula for the artifacts far from a small, radially symmetric object. More recent results are in [15–17]. These include the prediction of the location and frequency of the artifacts, qualitative analysis of the artifacts generated by various edges (e.g., flat, convex, and a corner), as well as their numerical illustrations.

In this paper we generalize the LRA to the analysis of view aliasing. We call it the Local Aliasing Analysis, or LAA. Our main result is Theorem 2.5, where a precise, quantitative formula describing aliasing artifacts is stated. The formula is asymptotic, it is established in the limit as the sampling rate $\epsilon \rightarrow 0$ (which is the same assumption as in [15–17]). Similarly to the LRA, the LAA is very flexible. In this paper we consider the generalized Radon transform in \mathbb{R}^2 and apply it

to functions with jump discontinuities across smooth, convex curves. Similarly to [18–22], we believe that the LAA is generalizable, and that it is capable of predicting aliasing artifacts for a wide range of integral transforms, conormal distributions f , and reconstruction operators.

The paper is organized as follows. In section 2 we describe the set-up, formulate the assumptions, and state the main result – Theorem 2.5. This theorem provides a simple formula that describes aliasing artifacts. The proof of the theorem is in section 3. Section 4.1 establishes a few useful properties of the function Ψ , in terms of which the artifacts are described. An algorithm for computing Ψ numerically is in Section 4.2. Section 5 contains numerical experiments with the classical and generalized Radon transforms. The latter integrates over circles. Details of implementation, which illustrate the use of the theorem, are provided. All experiments demonstrate a good match between reconstruction and prediction. Proofs of some lemmas are in appendix A.

2. PRELIMINARIES

2.1. Generalized Radon transform. Let $\Phi(x; \alpha, p)$ be a defining function for the generalized Radon transform \mathcal{R} :

$$(2.1) \quad \hat{f}(\alpha, p) = \int_{\mathcal{S}_{\alpha, p}} W(x; \alpha, p) f(x) dA, \quad \mathcal{S}_{\alpha, p} := \{x \in \mathbb{R}^2 : \Phi(x; \alpha, p) = 0\}, \alpha \in \Omega, p \in \mathbb{R},$$

where $W \in C^\infty(\mathbb{R}^2 \times \Omega \times \mathbb{R})$ is some (known) integration weight, dA is the length element on the curve $\mathcal{S}_{\alpha, p}$, and Ω is a small interval. As is well-known, $dA = (\det \hat{G}(x; \alpha, p))^{1/2} dx$, where \hat{G} is the Gram matrix

$$(2.2) \quad \hat{G} = \{G_{jk}\}_{j,k=1}^2, \quad G_{jk}(x; \alpha, p) = \frac{\partial \Phi(x; \alpha, p)}{\partial x_j} \frac{\partial \Phi(x; \alpha, p)}{\partial x_k}, \quad 1 \leq j, k \leq 2.$$

Similarly to the classical Radon transform, we think about α as the polar angle, and p as the affine variable. However, since we consider the generalized Radon transform, these variables admit many alternative interpretations.

Let \mathcal{S} be a C^∞ curve. We will compute a reconstruction in a small neighborhood of some point $x_0 \notin \mathcal{S}$. Let (α_*, p_0) be a pair such that $x_0 \in \mathcal{S}_{\alpha_*, p_0}$, and $\mathcal{S}_{\alpha_*, p_0}$ is tangent to \mathcal{S} at some $y_0 \in \mathcal{S}$. Let $H(y) = 0$ be an equation for \mathcal{S} in a neighborhood of y_0 , where H is smooth and $d_y H(y) \neq 0$, $y \in \mathcal{S}$. Multiplying H by a constant if necessary, we can assume that Φ satisfies the equations

$$(2.3) \quad \Phi(y_0; \alpha_*, p_0) = 0, \quad \vec{\Theta}_0 := d_y \Phi(y_0; \alpha_*, p_0) = d_y H(y_0), \quad \Phi(x_0; \alpha_*, p_0) = 0.$$

Let \mathcal{R}^* be a suitably truncated adjoint transform. Due to the fact that $\mathcal{R}^* \mathcal{R}$ is a PDO (this follows from assumptions 2.1 below, see e.g. [26] for similar arguments), we can restrict α to a small neighborhood $\Omega \ni \alpha_*$ when applying \mathcal{R}^* .

Assumptions 2.1 (Properties of Φ).

- Φ1. $\Phi \in C^\infty(\mathbb{R}^2 \times \Omega \times \mathbb{R})$, and $d_x \Phi(x; \alpha, p) \neq 0$ for any $x \in \mathcal{S}_{\alpha, p}$, $(\alpha, p) \in \Omega \times \mathbb{R}$;
- Φ2. Equations (2.3) hold;
- Φ3. The differentials $d_{\alpha, p} \Phi(x_0; \alpha_*, p_0)$ and $d_{\alpha, p} \Phi(y_0; \alpha_*, p_0)$ are linearly independent; and
- Φ4. One has

$$(2.4) \quad M \partial_p \Phi(x_0; \alpha_*, p_0) > 0, \quad M := (\vec{\Theta}_0^\perp \cdot \partial_y)^2 (H(y) - \Phi(y; \alpha_*, p_0))|_{y=y_0},$$

where $\vec{\Theta}_0^\perp$ is a unit vector orthogonal to $\vec{\Theta}_0$.

Assumption 2.1(Φ4) means that $\mathcal{S}_{\alpha_*, p_0 + \delta}$ intersects \mathcal{S} at two points near y_0 when $\delta > 0$, and does not intersect \mathcal{S} near y_0 – if $\delta < 0$. The requirement that the product

be positive is not restrictive. If the product is negative, we can flip the p -axis to make it positive. The essential requirement is that each factor be non-zero.

Let $\mathcal{P}(\alpha)$ be the function defined on Ω by the requirement that the curves $\mathcal{S}_{\alpha, \mathcal{P}(\alpha)}$, $\alpha \in \Omega$, be tangent to \mathcal{S} in a neighborhood of y_0 . Define \mathcal{P}_* by the equation $\Phi(x; \alpha, \mathcal{P}_*(\alpha, x)) \equiv 0$ for x near x_0 and $\alpha \in \Omega$. The following lemma is proven in appendix A.1

Lemma 2.2. *For some sufficiently small open set $U' \ni x_0$, one has*

$$(2.5) \quad \begin{aligned} \mathcal{P}(\alpha_*) &= p_0, \quad \mathcal{P}(\alpha) \in C^\infty(\Omega), \quad \mathcal{P}_* \in C^\infty(\Omega \times U'), \\ u_0 &:= d_x \mathcal{P}_*(\alpha_*, x_0) \neq 0, \quad \mu_0 := d_\alpha(\mathcal{P}_*(\alpha_*, x_0) - \mathcal{P}(\alpha_*)) \neq 0. \end{aligned}$$

2.2. Remaining assumptions and main result. Consider a function $f(x)$ on the plane, $x \in \mathbb{R}^2$. We suppose that

Assumptions 2.3 (Properties of f).

- F1. $\text{supp}(f) \subset U$ for some open set $U \ni y_0$ with $\text{diam}(U)$ sufficiently small;
- F2. There exist open sets D_\pm and functions $f_\pm \in C^\infty(\mathbb{R}^2)$ such that

$$(2.6) \quad \begin{aligned} f(x) &\equiv f_-(x), \quad x \in D_-, \quad f(x) \equiv f_+(x), \quad x \in D_+, \\ D_- \cap D_+ &= \emptyset, \quad D_- \cup D_+ = U \setminus \mathcal{S}; \end{aligned}$$

and

- F3. $\mathcal{S} \cap U$ is a C^∞ curve.

Thus, $\text{sing supp}(f) \subset \mathcal{S}$. In general, $f_-(x) \neq f_+(x)$, $x \in \mathcal{S}$, so f may have a jump discontinuity across \mathcal{S} . Note that whether $x_0 \in U$ or not is irrelevant. Also, when U shrinks towards y_0 , \mathcal{S} does not change. Thus, $\mathcal{S} \cap U$ is a small segment of \mathcal{S} around y_0 . With this understanding, in what follows we do not distinguish between \mathcal{S} and $\mathcal{S} \cap U$.

Similarly to [17], we consider semi-discrete data

$$(2.7) \quad \hat{f}_\epsilon(\alpha_k, p) := \int w_\epsilon(p-s) \hat{f}(\alpha_k, s) ds, \quad \alpha_k := k\Delta\alpha, \quad p \in \mathbb{R}, \quad w_\epsilon(t) := \epsilon^{-1}w(t/\epsilon),$$

where w is a smoothing kernel (e.g., the detector aperture function), $\Delta\alpha = \kappa\epsilon$, and $\kappa > 0$ is fixed. Also, we assume that the data has been filtered with respect to p by convolving it with a smooth filter with support of size $O(\epsilon)$. This is a realistic assumption, because sampling rates along α and p are usually of the same order of magnitude.

Assumptions 2.4 (Assumptions about the smoothing kernel w).

- SK1. $w \in C_0^\infty(\mathbb{R})$; and
- SK2. $\int w(p) dp = 1$.

Hence, the data (2.7) represent the integrals of f along thin strips around $\mathcal{S}_{\alpha_k, p}$, and their width ($= O(\epsilon)$) is determined by ϵ and the support of w . In the ideal case, where w is the Dirac δ -function, the data represent the integrals of f along $\mathcal{S}_{\alpha_k, p}$.

Reconstruction from the data is achieved by the formula

$$(2.8) \quad f_\epsilon^{\text{rec}}(x) = -\frac{\Delta\alpha}{2\pi} \sum_{\alpha_k \in \Omega} \frac{\omega(x, \alpha_k)}{\pi} \int \frac{\partial_p \hat{f}_\epsilon(\alpha_k, p)}{p - \mathcal{P}_*(x, \alpha_k)} dp, \quad x \in U',$$

where $\omega \in C^\infty(U' \times \Omega)$ is some weight function. This is a discretized (in α) version of the classical FBP inversion formula [27] adapted to the generalized Radon transform in \mathbb{R}^2 (e.g., as it was done in [26, 28]). The integral with respect to p , which is understood in the principal value sense, is the filtering step (the Hilbert transform). The exterior sum is a quadrature rule corresponding to the backprojection integral.

Introduce the following notation:

$$(2.9) \quad \begin{aligned} \psi(\hat{q}) &:= (1/2) \int_0^\infty w(\hat{q} + \hat{p}) \hat{p}^{-1/2} d\hat{p}, \quad k_* := \alpha_* / \Delta\alpha, \\ \Psi(h; a, k_*) &:= \sum_k [\psi(a(k - k_*)) + h] - \psi(a(k - k_*)), \end{aligned}$$

and

$$(2.10) \quad \begin{aligned} \Delta f(y_0) &= \lim_{\epsilon \rightarrow 0^+} (f(y_0 + \epsilon \vec{\Theta}_0) - f(y_0 - \epsilon \vec{\Theta}_0)), \\ \iota &:= -\operatorname{sgn}(\partial_p \Phi(x_0; \alpha_*, p_0)). \end{aligned}$$

Note that k_* is not necessarily an integer. The sign of ι is chosen so that $\iota \vec{\Theta}_0$ points towards the part of $\mathcal{S}_{\alpha_*, p_0 + \delta}$, $0 < \delta \ll 1$, located between its two intersection points with \mathcal{S} . Recall that M is defined in (2.4). Our main result is as follows.

Theorem 2.5. *Suppose $W \in C^\infty(\mathbb{R}^2 \times \Omega \times \mathbb{R})$, and $\omega \in C^\infty(U' \times \Omega)$ for some small open set $U' \ni x_0$. Under the assumptions 2.1, 2.3, and 2.4, one has*

$$(2.11) \quad \begin{aligned} \epsilon^{-1/2} (f_\epsilon^{rec}(x_0 + \epsilon \vec{x}) - f_\epsilon^{rec}(x_0)) &= c \Psi(u_0 \cdot \vec{x}; \mu_0 \kappa, k_*) + O(\epsilon^{1/2}), \quad \epsilon \rightarrow 0, \\ c &:= -\frac{\kappa \omega(x_0, \alpha_*) W(x_0; \alpha_*, p_0)}{\pi} \sqrt{\frac{2 \partial_p \Phi(x_0; \alpha_*, p_0)}{M}} \Delta f(x_0), \end{aligned}$$

where the $O(\epsilon^{1/2})$ term is uniform with respect to \vec{x} confined to any bounded set.

By Lemma 2.2, $u_0 \neq 0$, $\mu_0 \neq 0$. By linearity of the Radon transform, we can assume that the support of f is contained in a small neighborhood of y_0 (i.e., by shrinking U as much as necessary). By assumption 2.1(Φ4), shrinking U even more, we can assume that for any compact $K \subset U$, there exist $a_K, b_K > 0$ such that

$$(2.12) \quad \begin{aligned} \mathcal{S}_{\alpha, p} \cap K &= \emptyset \text{ for any } \alpha \in \Omega, |p - p_0| \geq a_K; \\ 1/b_K \leq |\partial_p \Phi(x; \alpha, p)| &\leq b_K \text{ for any } x \in \mathcal{S}_{\alpha, p}, \alpha \in \Omega, |p - p_0| \leq a_K. \end{aligned}$$

Then

$$(2.13)$$

$$\hat{f}(\alpha, p) = \varphi_1(\alpha)(p - \mathcal{P}(\alpha))_+^{1/2} + \varphi_2(\alpha, p)(p - \mathcal{P}(\alpha))_+^{3/2} + \varphi_3(\alpha, p), \quad \alpha \in \Omega, p \in \mathbb{R},$$

where $\varphi_1 \in C^\infty(\Omega)$, $\varphi_{2,3} \in C^\infty(\Omega \times \mathbb{R})$, and

$$(2.14) \quad \varphi_1(\alpha_*) = W(y_0; \alpha_*, p_0) \Delta f(y_0) 2 \sqrt{2 \partial_p \Phi(x_0; \alpha_*, p_0) / M}.$$

For the classical Radon transform this result is established in [29, 30]. For the generalized Radon transform it easily follows using assumptions 2.1(Φ1, Φ2) and (2.12) by applying the method of proof of Lemma 3.5 in [21].

Since $f(x)$ is compactly supported, $\hat{f}(\alpha, p)$ is compactly supported in p by (2.12). Hence we can assume that $\varphi_2(\alpha, p)$ is compactly supported as well, and

$$(2.15) \quad \varphi_3(\alpha, p) \equiv -\varphi_1(\alpha)(p - \mathcal{P}(\alpha))_+^{1/2}, \quad \alpha \in \Omega, |p| \geq c,$$

for some c .

3. PROOF OF THEOREM 2.5

The idea of the proof is to split \hat{f} into three terms using (2.13), substitute each of them one by one into (2.7), (2.8), and investigate the resulting expressions separately.

3.1. Beginning of proof. Estimate of the leading term. Replace $\hat{f}(\alpha, s)$ with $\varphi_1(\alpha)(s - \mathcal{P}(\alpha))_+^{1/2}$ in (2.7) and substitute into (2.8). After simple transformations we get

$$(3.1) \quad \begin{aligned} f_\epsilon^{\text{rec-1}}(x) &:= -\frac{\Delta\alpha}{2\pi\epsilon^{1/2}} \sum_{\alpha_k \in \Omega} \omega(x, \alpha_k) \varphi_1(\alpha_k) \psi((\mathcal{P}_*(\alpha_k, x) - \mathcal{P}(\alpha_k))/\epsilon), \\ \psi(\hat{q}) &:= (1/\pi) \int (\hat{p} - \hat{q})^{-1} \int w'(\hat{p} - \hat{s}) \hat{s}_+^{1/2} d\hat{s} d\hat{p}. \end{aligned}$$

After additional transformations with the help of the integral (3.7), ψ simplifies to the expression in (2.9). This gives

$$(3.2) \quad \begin{aligned} \psi(\hat{q}) &= 0, \quad \hat{q} > c; \\ \psi^{(n)}(\hat{q}) &= c_n(-\hat{q})^{-(1/2)-n} + O(|\hat{q}|^{-(3/2)-n}), \quad \hat{q} \rightarrow -\infty, n = 0, 1, 2, \dots, \end{aligned}$$

for some c and c_n .

Using the notation in (2.5) and (2.9) we formulate the following result

Lemma 3.1. *Under the assumptions of Theorem 2.5 one has*

$$(3.3) \quad \begin{aligned} \epsilon^{-1/2} (f_\epsilon^{\text{rec-1}}(x_0 + \epsilon\check{x}) - f_\epsilon^{\text{rec-1}}(x_0)) \\ = -\frac{\kappa\omega(x_0, \alpha_\star)\varphi_1(\alpha_\star)}{2\pi} \Psi(u_0 \cdot \check{x}; \mu_0\kappa, k_\star) + O(\epsilon^{1/2}), \end{aligned}$$

where the $O(\epsilon^{1/2})$ term is uniform with respect to \check{x} confined to any bounded set.

3.2. The second term. Similarly, replace $\hat{f}(\alpha, s)$ with $\varphi_2(\alpha, s)(s - \mathcal{P}(\alpha))_+^{3/2}$ in (2.7) and substitute into (2.8). After simple transformations we get with some c

$$(3.4) \quad \begin{aligned} f_\epsilon^{\text{rec-2}}(x) &:= c\epsilon \sum_{\alpha_k \in \Omega} \omega(x, \alpha_k) g_2(\mathcal{P}_*(\alpha_k, x), \mathcal{P}(\alpha_k), \alpha_k), \quad x = x_0 + \epsilon\check{x}, \\ g_2(p_*, q, \alpha) &:= \int (p - p_*)^{-1} \partial_p \int w_\epsilon(p - s) \varphi_2(\alpha, s) (s - q)_+^{3/2} ds dp, \\ |p_*|, |q| &\leq P := |p_0| + a_K, \end{aligned}$$

where $K := \text{supp}(f)$ (see the first line in (2.12)). For simplicity, the dependence of g_2 , φ_2 , and related functions on α will be omitted from notation. Rewrite g_2 as follows:

$$(3.5) \quad g_2(p_*, q) = \int w_\epsilon(p_* - p) \int (s - p)^{-1} \partial_s \left(\varphi_2(s) (s - q)_+^{3/2} \right) ds dp.$$

Using the results in [31, §8.3], we find

$$(3.6) \quad g_2(p_*, q) = \int w_\epsilon(p_* - p) \left(\varphi_{2,1}(p, q) (p - q)_+^{1/2} + \varphi_{2,2}(p, q) \right) dp$$

for some smooth and bounded $\varphi_{2,1}$ and $\varphi_{2,2}$. The same result can be obtained by elementary means using the integral (see [32, Equations 2.2.4.25 and 2.2.4.26])

$$(3.7) \quad \int (s - \rho)^{-1} s_+^{-1/2} ds = \pi \rho_-^{-1/2},$$

writing

$$(3.8) \quad \int_0^\infty \frac{\varphi(s)}{s^{1/2}(s - \rho)} ds = \varphi(\rho) \int_0^\infty \frac{ds}{s^{1/2}(s - \rho)} + \int_0^\infty \frac{\varphi(s) - \varphi(\rho)}{s - \rho} s^{-1/2} ds,$$

and substituting $\rho = p - q$, $\varphi(s) = s[(3/2)\varphi_2(s + q) + s\varphi'_2(s + q)]$.

From (3.6) it follows that

$$(3.9) \quad \begin{aligned} & |g_2(p_* + \Delta p_*, q) - g_2(p_*, q)| \\ & \leq O(|\Delta p_*|) + c \max_{|p| \leq c\epsilon} \left| (p_* - q + \Delta p_* + p)_-^{1/2} - (p_* - q + p)_-^{1/2} \right| \end{aligned}$$

for some c . Recall that in (3.9)

$$(3.10) \quad p_* - q = \mathcal{P}_*(\alpha_k, x) - \mathcal{P}(\alpha_k), \quad \Delta p_* = \mathcal{P}_*(\alpha_k, x) - \mathcal{P}_*(\alpha_k, x_0), \quad p = O(\epsilon),$$

where $x = x_0 + \epsilon \ddot{x}$. Since $\mu_0 \neq 0$ (cf. (2.5)), we have $|\mathcal{P}_*(\alpha, x_0) - \mathcal{P}(\alpha)| \geq c|\alpha - \alpha_*|$ for any $\alpha \in \Omega$ and some $c > 0$. Therefore, there exists $c_1 > 0$ such that whenever $|\alpha - \alpha_*| \geq c_1 \epsilon$ and $\epsilon > 0$ is sufficiently small, the expressions $(p_* - q + \Delta p_* + p)_-^{1/2}$ and $(p_* - q + p)_-^{1/2}$ are either both zero or both nonzero. When they are both nonzero, the magnitude of their difference equals

$$(3.11) \quad \frac{|\Delta p_*|}{|p_* - q + \Delta p_* + p|^{1/2} + |p_* - q + p|^{1/2}} \leq \frac{c\epsilon}{|\alpha - \alpha_*|^{1/2}}, \quad |\alpha - \alpha_*| \geq c_1 \epsilon,$$

for some c . Also, there are finitely many k (close to k_*) such that $|\alpha_k - \alpha_*| < c_1 \epsilon$. For those k , the same difference is $O(\epsilon^{1/2})$.

Using (3.9) and (3.11) in (3.4), we find similarly to (2.11):

$$(3.12) \quad \begin{aligned} & \epsilon^{-1/2} (f_\epsilon^{\text{rec-2}}(x_0 + \epsilon \ddot{x}) - f_\epsilon^{\text{rec-2}}(x_0)) \\ & = O(\epsilon^{1/2}) + O(\epsilon^{1/2}) \left[O(\epsilon^{1/2}) + \sum_{1 \leq k \leq O(1/\epsilon)} \frac{O(\epsilon)}{(k\epsilon)^{1/2}} \right] = O(\epsilon^{1/2}). \end{aligned}$$

The first $O(\epsilon^{1/2})$ term on the right in (3.12) absorbs the contributions, which arise due to the x -dependence of ω in (3.4) and due to the $O(|\Delta p_*|) = O(\epsilon)$ term in (3.9). Here we use that $|\omega(x_0 + \epsilon \ddot{x}, \alpha) - \omega(x_0, \alpha)| \leq c\epsilon$ and $|g_2(p_*, q, \alpha)| \leq c$ for some c and all $\alpha \in \Omega$, $|p_*|, |q| \leq P$. Recall that φ_2 is compactly supported.

3.3. The third term. Finally, replace $\hat{f}(\alpha, s)$ with $\varphi_3(\alpha, s)$ in (2.7) and substitute into (2.8). Recall that φ_3 is not necessarily compactly supported in s (cf. (2.15)) and

$$(3.13) \quad \partial_s^l \varphi_3(\alpha, s) = O(|s|^{(1/2)-l}), \quad s \rightarrow \infty, \quad \alpha \in \Omega, \quad l = 0, 1, 2,$$

where the big- O term is uniform in α . Similarly to (3.4) and (3.5), we find

$$(3.14) \quad \begin{aligned} f_\epsilon^{\text{rec-3}}(x) & := c\epsilon \sum_{\alpha_k \in \Omega} \omega(x, \alpha_k) g_3(\mathcal{P}_*(\alpha_k, x), \alpha_k), \\ g_3(p_*, \alpha) & := \int (p - p_*)^{-1} \partial_p \int w_\epsilon(p - s) \varphi_3(\alpha, s) ds dp \\ & = \int w_\epsilon(-p) \int s^{-1} \partial_s \varphi_3(\alpha, s + p + p_*) ds dp, \quad |p_*| \leq P. \end{aligned}$$

The following lemma is proven in appendix A.3.

Lemma 3.2. *One has*

$$(3.15) \quad \int s^{-1} \partial_s [\varphi_3(\alpha, s + q + \Delta q) - \varphi_3(\alpha, s + q)] ds = O(|\Delta q|), \quad \Delta q \rightarrow 0,$$

uniformly in $\alpha \in \Omega$, $|q| \leq c$, for any c .

Using Lemma 3.2, the analogue of (3.9) becomes

$$(3.16) \quad \begin{aligned} & |g_3(p_* + \Delta p_*, \alpha) - g_3(p_*, \alpha)| \\ & \leq c \max_{|p| \leq c\epsilon} \left| \int s^{-1} \partial_s [\varphi_3(\alpha, s + p + p_* + \Delta p_*) - \varphi_3(\alpha, s + p + p_*)] ds \right| \\ & = O(|\Delta p_*|) = O(\epsilon), \quad \alpha \in \Omega, \end{aligned}$$

for some c . Hence, we obtain similarly to (3.12):

$$(3.17) \quad \epsilon^{-1/2}(f_\epsilon^{\text{rec-3}}(x_0 + \epsilon\check{x}) - f_\epsilon^{\text{rec-3}}(x_0)) = O(\epsilon^{1/2}).$$

Combining (2.11), (2.14), (3.12), (3.17), and using that $f_\epsilon^{\text{rec}} = f_\epsilon^{\text{rec-1}} + f_\epsilon^{\text{rec-2}} + f_\epsilon^{\text{rec-3}}$, we finish the proof of Theorem 2.5.

4. A MORE DETAILED LOOK AT THE FUNCTION Ψ

4.1. Properties of the function Ψ . Theorem 2.5 shows that the function Ψ defined in (2.9) plays a key role in the description of the aliasing artifact. Here we prove some of the properties of Ψ . In this section k_* denotes any real number rather than the specific value defined in (2.9).

Lemma 4.1. *One has*

$$(4.1) \quad \Psi(h; a, k_* + 1) = \Psi(h; a, k_*), \quad \Psi(h + a; a, k_*) = \Psi(h; a, k_*) \quad \forall h, a, k_* \in \mathbb{R}.$$

Proof. The first statement is obvious. To prove the second statement, fix some $c \gg 1$ and shift the index of summation $k' = k + 1$ in (2.9):

$$(4.2) \quad \Psi(h + a; a, k_*) = \sum_{k' \leq c} [\psi(a(k' - k_*) + h) - \psi(a(k' - 1 - k_*))].$$

At first glance, to finish the proof we can just change back $k = k' - 1$ in the second ψ . This does not work, since each of the sums taken separately is divergent (cf. (3.2)). Hence we argue differently. We have for any $N \gg 1$:

$$(4.3) \quad \begin{aligned} \Psi(h + a; a, k_*) &= \sum_{k'=-N}^c [\psi(a(k' - k_*) + h) - \psi(a(k' - 1 - k_*))] + O(N^{-1/2}) \\ &= \sum_{k'=-N}^c [\psi(a(k' - k_*) + h) - \psi(a(k' - k_*))] - \psi(a(N - 1 - k_*)) \\ &\quad + O(N^{-1/2}) = \Psi(h; a, k_*) + O(N^{-1/2}), \quad N \rightarrow \infty. \end{aligned}$$

The desired assertion now follows. \square

Lemma 4.2. *If $w \in C_0^\infty(\mathbb{R})$, one has*

$$(4.4) \quad \Psi(h; a, k_*) = O(|a|^{-\infty}), \quad a \rightarrow 0,$$

uniformly in $h, k_ \in \mathbb{R}$.*

Proof. We will need the following simple lemma, which is proven in appendix A.4.

Lemma 4.3. *Suppose $g \in C^\infty(\mathbb{R})$, $g^{(n)}(t) = O(|t|^a)$, $t \rightarrow \infty$, for some $a < -1$ and any $n = 0, 1, 2, \dots$, and $\int g(x)dx = 0$. Then*

$$(4.5) \quad \sum_k g(\epsilon(k - k_*)) = O(\epsilon^{-\infty}), \quad \epsilon \rightarrow 0,$$

uniformly with respect to $k_ \in \mathbb{R}$.*

Set $g(t) = \Delta\psi(t; h)$, where

$$(4.6) \quad \Delta\psi(t; h) := \psi(t + h) - \psi(t).$$

The dependence of g on h is omitted for simplicity. As is easily seen, g satisfies the assumptions of Lemma 4.3. Indeed, due to (4.1), we can assume $h \in [0, a)$,

$k_* \in [0, 1]$. From (3.2), $|\partial_t^n \Delta\psi(t; h)| \leq c_n(1 + |t|)^{-3/2}$, $n = 0, 1, 2, \dots$, for some c_n independent of $h \in [0, 1]$. Furthermore, for some $c > 0$,

$$(4.7) \quad \begin{aligned} \int \Delta\psi(t; h) dt &= \int_{-N}^c \Delta\psi(t; h) dt + O(N^{-1/2}) \\ &= - \int_{-N}^{h-N} \psi(t) dt + O(N^{-1/2}) = O(N^{-1/2}), \quad N \rightarrow \infty. \end{aligned}$$

Application of Lemma 4.3 to g with $\epsilon = a$ proves the desired assertion. The uniformity with respect to h is obvious from the proof of Lemma 4.3 (by noticing that the estimates for $A_j(\epsilon)$ are uniform with respect to h). \square

4.2. Computing Ψ numerically. Numerically, we compute Ψ using the following approach. In our experiments

$$(4.8) \quad w(t) = (15/16)(1 - t^2)_+^2.$$

First, $\psi(t)$ is computed by analytically evaluating the integral in (2.9). Then we compute $\Delta\psi$. For moderate values of t we use (4.6) directly. For $t \ll -1$ we use

$$(4.9) \quad \Delta\psi(t; h) \approx h/(4|t|^{1.5}).$$

Finally, we write

$$(4.10) \quad \Psi(h; a, k_*) \approx \sum_{k=-N+1}^c \Delta\psi(a(k - k_*); h) + \frac{h}{4|a|^{1.5}} \sum_{k=N}^{\infty} k^{-1.5},$$

where $c > 0$ is selected so that $\Delta\psi(a(k - k_*); h) = 0$ for all $k > c$ and $h \in [0, a]$, and $N \gg 1$. The last sum is estimated using the asymptotic formula for the Hurwitz Zeta Function [33, Equation (1.1)]

$$(4.11) \quad \zeta(s, r) := \sum_{k=0}^{\infty} (k + r)^{-s} = \frac{r^{1-s}}{s-1} + \frac{r^{-s}}{2} + O(r^{-(s+1)}), \quad r \rightarrow +\infty,$$

where $s = -3/2$ and $r = N$. The plots of $\Psi(ah'; a, k_*)$, $0 \leq h' \leq 1$, for the values $a = 1, 2, 4$ and $k_* = 1/3$ are shown in Figure 1.

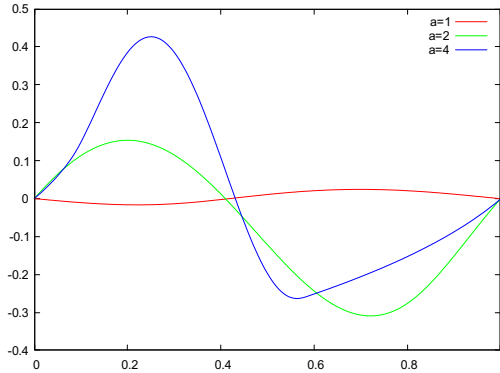


FIGURE 1. Plots of $\Psi(ah'; a, k_*)$ for three values of a . The variable h' is on the horizontal axis.

In agreement with Lemma 4.2, we see that $\Psi(ah'; a, k_*)$ decays rapidly as $a \rightarrow 0$.

5. NUMERICAL EXPERIMENTS

5.1. Classical Radon transform. In this subsection we experiment with the classical Radon transform (CRT), which integrates over lines:

$$(5.1) \quad \hat{f}(\alpha, p) = \int_{S_{\alpha, p}} f(x) dx, \quad \vec{\alpha} = (\cos \alpha, \sin \alpha), \quad S_{\alpha, p} := \{x \in \mathbb{R}^2 : \alpha \cdot x = p\}.$$

Obviously, we can set $\Phi(x; \alpha, p) = \alpha \cdot x - p$. This gives (cf. (2.4), (2.10), (2.11))

$$(5.2) \quad \partial_p \Phi(x_0; \alpha_*, p_0) = -1, \quad \iota = 1, \quad M = (\vec{\Theta}_0^\perp \cdot \partial_y)^2 H(y)|_{y=y_0} < 0,$$

i.e. $|M|$ is the curvature of \mathcal{S} at y_0 . Together with $\vec{\Theta}_0 = d_y H(y_0)$, (5.2) implies that, as expected, $\vec{\Theta}_0$ points towards the center of curvature of \mathcal{S} at y_0 .

Reconstruction uses (2.8):

$$(5.3) \quad \begin{aligned} f_\epsilon^{\text{rec}}(x) &= -\frac{\Delta \alpha}{2\pi} \sum_{|\alpha_k| \leq \pi/2} \frac{1}{\pi} \int \frac{\partial_p \hat{f}_\epsilon(\alpha_k, p)}{p - \mathcal{P}_*(x, \alpha_k)} dp, \quad \mathcal{P}_*(x, \alpha) \equiv \vec{\alpha} \cdot x, \\ \hat{f}_\epsilon(\alpha_k, p) &= \int w_\epsilon(p - \rho) \hat{f}(\alpha_k, \rho) d\rho, \quad \alpha_k = -(\pi/2) + (\pi/N_\alpha)(k + \delta), \end{aligned}$$

and w is the same as in (4.8). Note that the weights in both the Radon transform and the inversion formula are set to 1: $W(x; \alpha, p) \equiv 1$, $\omega(x, \alpha) \equiv 1$.

The function f is the characteristic function of the disk centered at the origin with radius r . Thus, $\mathcal{S} = \{x \in \mathbb{R}^2 : |x| = r\}$ and $M = -1/r$.

At a given x , aliasing arises due to the parts of \mathcal{S} where the lines $S_{\alpha, p} \ni x$ are tangent to \mathcal{S} . For $|x| > r$, two such lines exist. We pick $x_0 = (r, h)$ and find two pairs (α_*, p_0) with the required properties. Clearly, one of the pairs is $(\alpha_* = 0, p_0 = r)$, and the other - $(\alpha_* = 2 \tan^{-1}(h/r) - \pi, p_0 = -r)$. For reconstructions we use $r = 5$ and $x_0 = (5, 7)$. To better illustrate the aliasing artifact we also reconstruct a small region of interest (ROI), which is a square centered at x_0 with side length 40ϵ .

For computations we also need u_0 and μ_0 (cf. (2.11)). They follow easily from (2.5):

$$(5.4) \quad u_0 = \vec{\alpha}_*, \quad \mu_0 = \vec{\alpha}_*^\perp \cdot (x_0 - y_0),$$

where y_0 is the point where S_{α_*, p_0} is tangent to \mathcal{S} .

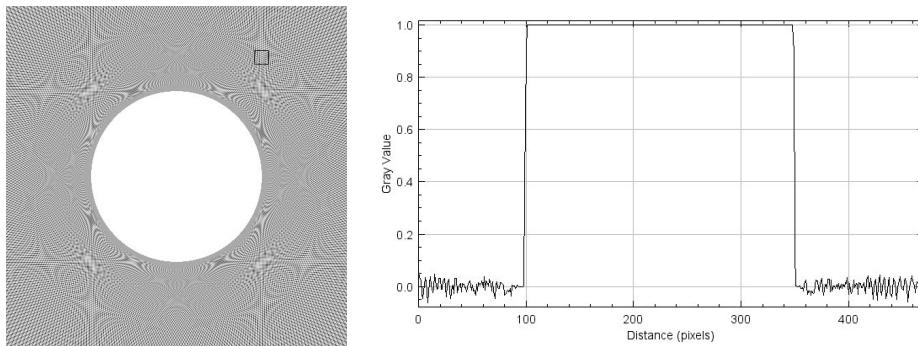


FIGURE 2. CRT reconstruction of the region $|x_1|, |x_2| \leq 10$: $\epsilon = 0.02$, $N_\alpha = 200$, $\delta = 0.03$. Left: global reconstruction, right: profile of the reconstruction through the center.

In the first experiment, $\epsilon = 0.02$, $N_\alpha = 200$, and in the second: $\epsilon = 0.01$, $N_\alpha = 400$. Since the direction $\alpha_* = 0$ is special, we use a non zero shift δ in (5.3) for additional generality. The results are shown in Figures 2 – 7.

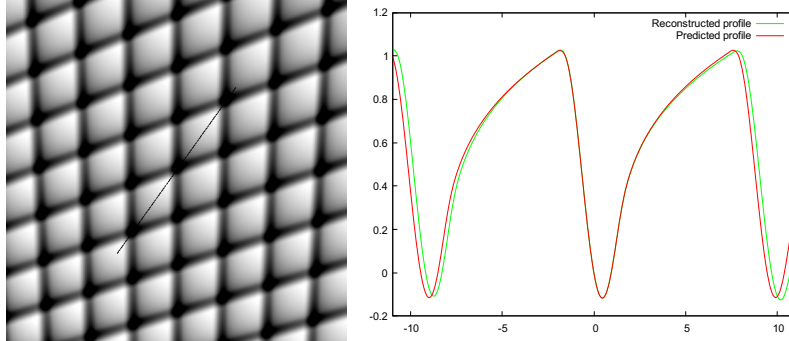


FIGURE 3. ROI CRT reconstruction: $\epsilon = 0.02$, $N_\alpha = 200$, $\delta = 0.03$. The ROI is the square shown in Figure 2. Left: reconstructed ROI, right: reconstructed (green) and predicted (red) profiles along the line segment $x = x_0 + \epsilon h \vec{\Theta}$, $|h| \leq 11$, shown on the left. The variable h is on the horizontal axis.

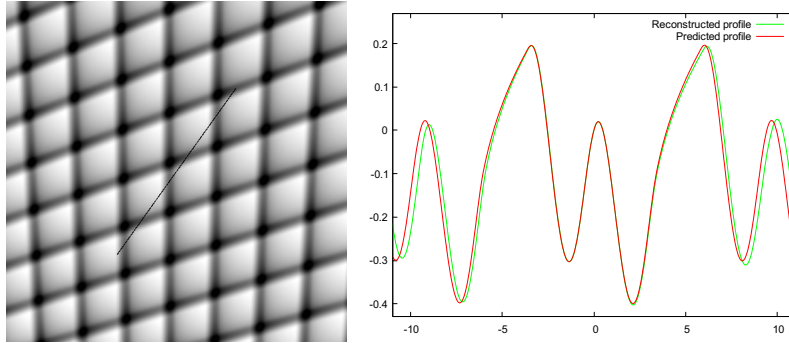


FIGURE 4. ROI CRT reconstruction: $\epsilon = 0.02$, $N_\alpha = 200$, $\delta = 0.2$. The ROI is the square shown on the left in Figure 2. Left: reconstructed ROI, right: reconstructed (green) and predicted (red) profiles along the line segment $x = x_0 + \epsilon h \vec{\Theta}$, $|h| \leq 11$, shown on the left. The variable h is on the horizontal axis.

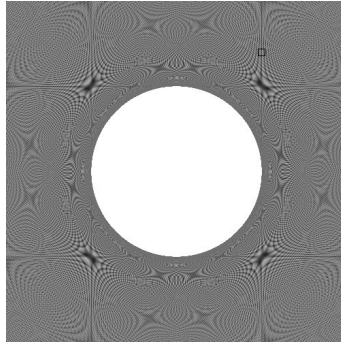


FIGURE 5. CRT reconstruction of the region $|x_1|, |x_2| \leq 10$: $\epsilon = 0.01$, $N_\alpha = 400$, $\delta = 0.03$.

Figure 2 (left panel) shows the reconstructed region $|x_1|, |x_2| \leq 10$ with $\epsilon = 0.02$ and $N_\alpha = 200$. The left panel shows also the ROI (a small square). The right panel shows a line profile through the origin to confirm the accuracy of reconstruction.

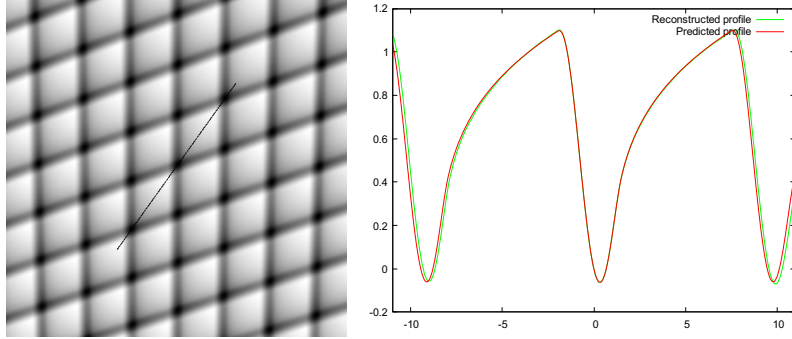


FIGURE 6. ROI CRT reconstruction: $\epsilon = 0.01$, $N_\alpha = 400$, $\delta = 0.03$. The ROI is the square shown on the left in Figure 5. Left: reconstructed ROI, right: reconstructed (green) and predicted (red) profiles along the line segment $x = x_0 + \epsilon h \vec{\Theta}$, $|h| \leq 11$, shown on the left. The variable h is on the horizontal axis.

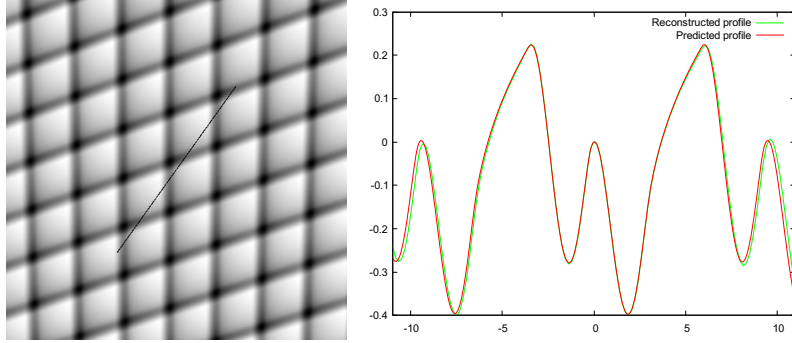


FIGURE 7. ROI CRT reconstruction: $\epsilon = 0.01$, $N_\alpha = 400$, $\delta = 0.2$. The ROI is the square shown on the left in Figure 5. Left: reconstructed ROI, right: reconstructed (green) and predicted (red) profiles along the line segment $x = x_0 + \epsilon h \vec{\Theta}$, $|h| \leq 11$, shown on the left. The variable h is on the horizontal axis.

Figure 3 shows the reconstructed ROI with $\delta = 0.03$. The right panel shows the profiles of the reconstructed difference $\epsilon^{-1/2}(f_\epsilon^{\text{rec}}(x) - f_\epsilon^{\text{rec}}(x_0))$ (green) and the prediction given by the main term on the right in (2.11) (red) along the line segment $x = x_0 + \epsilon h \vec{\Theta}$, $|h| \leq 11$, where $\vec{\Theta} = x_0/|x_0|$. The line segment is indicated on the left panel. The values of h are on the horizontal axis of the profile. Similarly, Figure 4 shows the reconstructed ROI and line profiles for the same line segment when $\delta = 0.2$.

Figure 5 shows the reconstructed region $|x_1|, |x_2| \leq 10$ with $\epsilon = 0.01$ and $N_\alpha = 400$. The ROI is indicated on the left panel. Recall that the size of the ROI is proportional to ϵ . Figure 6 shows the ROI and the corresponding line profiles for $\delta = 0.03$. Similarly, Figure 7 shows the reconstructed ROI and line profiles when $\delta = 0.2$. In both cases, the vector $\vec{\Theta}$ and the range of h that determine the line segment are the same as before.

Comparing Figure 3 with Figure 6 and Figure 4 with Figure 7, we see that reducing ϵ and $\Delta\alpha$ improves the match between the reconstruction and prediction.

5.2. Generalized Radon transform. In this subsection we experiment with the generalized Radon transform (GRT), which integrates over circles with radius $\rho > 0$

and centers on the circle $|x| = R$:

$$(5.5) \quad (\mathcal{R}f)(\alpha, \rho) = \hat{f}(\alpha, \rho) = \int_{S_{\alpha, \rho}} f(x) dx, \quad \vec{\alpha} = (\cos \alpha, \sin \alpha),$$

$$\Phi(x; \alpha, \rho) := |x - R\vec{\alpha}| - \rho, \quad S_{\alpha, \rho} := \{x \in \mathbb{R}^2 : |x - R\vec{\alpha}| = \rho\}.$$

The value of R is fixed. Therefore

$$(5.6) \quad \partial_\rho \Phi(x; \alpha, \rho) = -1, \quad d_x \Phi(x; \alpha, \rho) = \frac{x - R\vec{\alpha}}{|x - R\vec{\alpha}|}, \quad \iota = 1,$$

$$M = (\vec{\Theta}_0^\perp \cdot \partial_y)^2 H(y)|_{y=y_0} - (1/\rho_0) < 0.$$

Reconstruction is achieved using a straightforward modification of (2.8)

$$(5.7) \quad f_\epsilon^{\text{rec}}(x) = -\frac{\Delta\alpha}{2\pi} \sum_{\alpha_k \in \Omega} \frac{1}{\pi} \int \frac{\partial_\rho \hat{f}_\epsilon(\alpha_k, \rho)}{p - \mathcal{P}_*(x, \alpha_k)} d\rho, \quad \mathcal{P}_*(x, \alpha) \equiv |x - R\vec{\alpha}|,$$

$$\hat{f}(\alpha_k, \rho) = \int w_\epsilon(\rho - \rho') \hat{f}(\alpha_k, \rho') d\rho', \quad \alpha_k = (2\pi/N_\alpha)k, \quad w(\rho) = (1 - \rho^2)_+^2,$$

i.e. w is the same as in (4.8). Clearly, the reconstruction is not theoretically exact anymore. But it preserves the strength of the singularities (in the Sobolev scale). Again, the weights in both the Radon transform and the inversion formula are set to 1: $W(x; \alpha, \rho) \equiv 1$, $\omega(x, \alpha) \equiv 1$.

The function f is the characteristic function of the disk centered at x_c with radius r . Thus, $\mathcal{S} = \{x \in \mathbb{R}^2 : |x - x_c| = r\}$.

At a given x_0 , aliasing arises due to the parts of \mathcal{S} where various $S_{\alpha, \rho} \ni x_0$ are tangent to \mathcal{S} . To find all such (α, ρ) we should solve the equation

$$(5.8) \quad |x_c - R\vec{\alpha}| - |x_0 - R\vec{\alpha}| = \pm r$$

for α and set $\rho = |x_0 - R\vec{\alpha}|$. Generally, up to four solutions (α, ρ) (i.e., up to four circles $S_{\alpha, \rho}$) can exist. To simplify the experiment, we reverse the argument. We pick some pair (α_*, ρ_0) such that S_{α_*, ρ_0} is tangent to \mathcal{S} at some y_0 , and then select some $x_0 \in S_{\alpha_*, \rho_0}$. To be specific, we select a '+' in (5.8), i.e. ρ_0 satisfies $|x_c - R\vec{\alpha}| = r + \rho_0$. This implies that $M = -[(1/r) + (1/\rho_0)]$, and $\vec{\Theta}_0 = (y_0 - R\vec{\alpha}_*)/|y_0 - R\vec{\alpha}_*|$ points towards the center of curvature of \mathcal{S} at y_0 .

To illustrate aliasing only from the place where S_{α_*, ρ_0} is tangent to \mathcal{S} we select Ω to be a sufficiently small neighborhood of α_* . Similarly to (5.4),

$$(5.9) \quad u_0 = \frac{x_0 - R\vec{\alpha}_*}{|x_0 - R\vec{\alpha}_*|}, \quad \mu_0 = -R\vec{\alpha}_*^\perp \cdot \left(u_0 - \frac{x_c - R\vec{\alpha}_*}{|x_c - R\vec{\alpha}_*|} \right) = -R\vec{\alpha}_*^\perp \cdot (u_0 - \vec{\Theta}_0).$$

For reconstructions we use

$$(5.10) \quad R = 5, \quad x_c = (1, 1), \quad r = 2, \quad (\alpha_*, \rho_0) = (0.53\pi, 2.24), \quad x_0 = (-1.42, 2.95),$$

$$\Omega := [\alpha_* - \pi/4, \alpha_* + \pi/4].$$

In the first reconstruction, $\epsilon = 10^{-2}$, $N_\alpha = 500$, and in the second: $\epsilon = 0.5 \cdot 10^{-2}$, $N_\alpha = 1000$. The results are shown in Figures 8 and 9, respectively. The left panels show the limited angle reconstruction of the region $|x_1|, |x_2| \leq 4$. The middle panels show the limited angle reconstruction of an ROI. The ROI is a small square centered at x_0 with side length 40ϵ , the ROI is shown on the left panel. The right panels show the profiles of the reconstructed difference $\epsilon^{-1/2}(f_\epsilon^{\text{rec}}(x) - f_\epsilon^{\text{rec}}(x_0))$ (green) and the prediction given by the main term on the right in (2.11) (red) along the line segment $x = x_0 + eh\vec{\Theta}$, $|h| \leq 6$, shown in the middle panel. The values of h are on the horizontal axis of the profiles. The unit vector $\vec{\Theta}$ is chosen to be orthogonal to S_{α_*, ρ_0} at x_0 (i.e., $\vec{\Theta}$ and u_0 are parallel). In the experiments we set $\vec{\Theta} = -u_0$.

As is seen, reducing ϵ and $\Delta\alpha$ improves the match between the reconstruction and prediction.

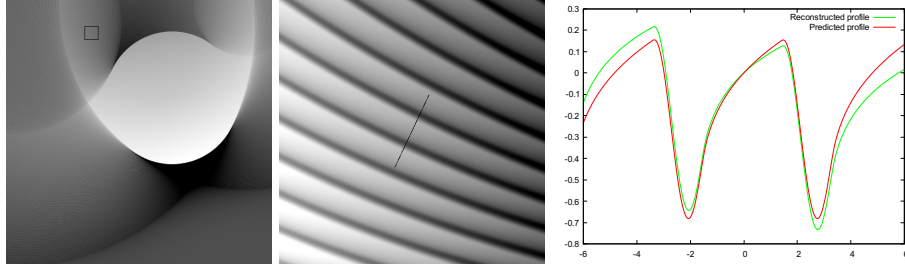


FIGURE 8. Limited angle GRT reconstruction: $\epsilon = 0.01$, $N_\alpha = 500$. Left: global reconstruction, middle: reconstruction inside the square ROI shown on the left, right: profiles of the reconstruction (green) and prediction (red) along the line segment $x = x_0 + \epsilon h \vec{\Theta}$, $|h| \leq 6$, shown in the middle. The variable h is on the horizontal axis.

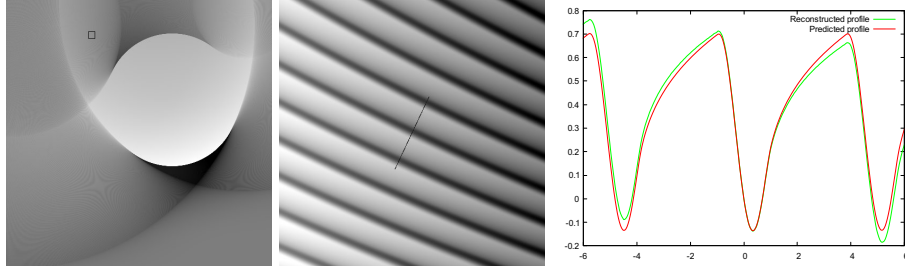


FIGURE 9. Limited angle GRT reconstruction: $\epsilon = 0.005$, $N_\alpha = 1000$. Left: global reconstruction, middle: reconstruction inside the square ROI shown on the left, right: profiles of the reconstruction (green) and prediction (red) along the line segment $x = x_0 + \epsilon h \vec{\Theta}$, $|h| \leq 6$, shown in the middle. The variable h is on the horizontal axis.

APPENDIX A. PROOFS OF LEMMAS

A.1. Proof of Lemma 2.2. The property $\mathcal{P}(\alpha_*) = p_0$ follows from assumption 2.1(Φ2). Recall that $H(y) = 0$ is a local equation of \mathcal{S} (cf. (2.3) and the paragraph preceding it). To find $\mathcal{P}(\alpha)$, we solve

$$(A.1) \quad H(y) = 0, \quad \Phi(y; \alpha, p) = 0, \quad \lambda d_y H(y) = d_y \Phi(y; \alpha, p)$$

for p in terms of α near (y_0, α_*, p_0) . Assumptions 2.1(Φ1, Φ2, Φ4) and the Implicit Function Theorem imply that $\mathcal{P}(\alpha)$ is smooth. Likewise, (2.12) implies that $\mathcal{P}_* \in C^\infty(\Omega \times U')$ for a sufficiently small open $U' \ni x_0$. From the definition of \mathcal{P}_* we get

$$(A.2) \quad \partial_x \Phi(x_0; \alpha_*, p_0) + d_p \Phi(x_0; \alpha_*, p_0) \partial_x \mathcal{P}_*(\alpha_*, x_0) = 0,$$

and assumptions 2.1(Φ1, Φ4) imply that $u_0 \neq 0$. Finally, differentiate $\Phi(y; \alpha, p) \equiv 0$ with respect to α , where y and p are functions of α :

$$(A.3) \quad d_y \Phi(y; \alpha, \mathcal{P}(\alpha)) (\partial y / \partial \alpha) + \partial_\alpha \Phi(y; \alpha, \mathcal{P}(\alpha)) + d_p \Phi(y; \alpha, \mathcal{P}(\alpha)) \mathcal{P}'(\alpha) \equiv 0.$$

Since $\mathcal{S}_{\alpha,p}$ is tangent to \mathcal{S} , the first term on the left in (A.3) equals zero. Similarly to (A.2),

$$(A.4) \quad \partial_\alpha \Phi(x_0; \alpha_\star, p_0) + d_p \Phi(x_0; \alpha_\star, p_0) \partial_\alpha \mathcal{P}_*(\alpha_\star, x_0) = 0,$$

and appealing to assumption 2.1(Φ3) proves that $\mu_0 \neq 0$.

A.2. Proof of Lemma 3.1.

Denote

$$(A.5) \quad H(x, \alpha, \epsilon) := \frac{\mathcal{P}_*(\alpha, x) - \mathcal{P}(\alpha)}{\epsilon}, \quad x = x_0 + \epsilon \check{x}, \alpha \in \Omega.$$

Since $\mu_0 \neq 0$ (cf. (2.5)), we have $|\mathcal{P}_*(\alpha, x_0) - \mathcal{P}(\alpha)| \geq c|\alpha - \alpha_\star|$ for any $\alpha \in \Omega$ and some $c > 0$. Hence

$$(A.6) \quad |H(x, \alpha_k, \epsilon)| \geq c_1 + c_2 |k - k_\star|, \quad \text{for all } |\check{x}| \leq c, \alpha_k \in \Omega,$$

for some $c, c_1, c_2 > 0$, and all $\epsilon > 0$ sufficiently small. From (3.1),

$$(A.7) \quad \begin{aligned} f_\epsilon^{\text{rec-1}}(x_0 + \epsilon \check{x}) - f_\epsilon^{\text{rec-1}}(x_0) &= -\frac{\Delta \alpha}{2\pi \epsilon^{1/2}} J + O(\epsilon), \\ J &:= \sum_{\alpha_k \in \Omega} \omega(x_0, \alpha_k) \varphi_1(\alpha_k) [\psi(H(x_0 + \epsilon \check{x}, \alpha_k, \epsilon)) - \psi(H(x_0, \alpha_k, \epsilon))]. \end{aligned}$$

The $O(\epsilon)$ term on the right in (A.7) denotes the contribution, which arises due to the x -dependence of ω in (3.1). Here we use (3.2) with $n = 0$, (A.6), and that for some c and all \check{x} in a bounded set:

$$(A.8) \quad |\omega(x_0 + \epsilon \check{x}, \alpha) - \omega(x_0, \alpha)| \leq c\epsilon, \quad |\varphi_1(\alpha)| \leq c, \quad \alpha \in \Omega.$$

Using (2.5) gives

$$(A.9) \quad H(x_0 + \epsilon \check{x}, \alpha, \epsilon) = H(x_0, \alpha, \epsilon) + u_0 \cdot \check{x} + O(\epsilon + |\alpha - \alpha_\star|).$$

Also, $|\omega(x_0, \alpha) \varphi_1(\alpha)| \leq c$ for some c and all $\alpha \in \Omega$. Therefore, by (3.2) with $n = 1$ and (A.6),

$$(A.10) \quad \begin{aligned} \sum_{|k| \leq O(1/\epsilon)} \omega(x_0, \alpha_k) \varphi_1(\alpha_k) [\psi(H(x_0 + \epsilon \check{x}, \alpha_k, \epsilon)) - \psi(H(x_0, \alpha_k, \epsilon) + u_0 \cdot \check{x})] \\ = \sum_{|k| \leq O(1/\epsilon)} \psi'(H(x_0, \alpha_k, \epsilon) + O(1)) O(\epsilon + \epsilon |k - k_\star|) \\ = O(\epsilon) \sum_{|k| \leq O(1/\epsilon)} \frac{1 + |k - k_\star|}{c_1 + c_2 |k - k_\star|^{3/2}} = O(\epsilon^{1/2}). \end{aligned}$$

This implies

$$(A.11) \quad J = \sum_{\alpha_k \in \Omega} \omega(x_0, \alpha_k) \varphi_1(\alpha_k) \Delta \psi(H(x_0, \alpha_k, \epsilon); h) + O(\epsilon^{1/2}), \quad h := u_0 \cdot \check{x}.$$

Recall that $\Delta \psi$ is defined in (4.6).

Furthermore,

$$(A.12) \quad H(x_0, \alpha_k, \epsilon) = \mu_0 \frac{\alpha_k - \alpha_\star}{\epsilon} + R_k, \quad R_k = O(\epsilon(k - k_\star)^2).$$

Denote, for simplicity, $a_k = \mu_0 \kappa(k - k_\star)$. Then

$$(A.13) \quad \Delta \psi(a_k + R_k; h) - \Delta \psi(a_k; h) = R_k \Delta \psi'(a_k + \xi_k; h),$$

where $|\xi_k| \leq |R_k|$. We can assume that Ω is sufficiently small, so that

$$(A.14) \quad |\mu_0(\alpha_k - \alpha_\star) + \epsilon R_k| \geq c|\alpha_k - \alpha_\star|, \quad \forall \alpha_k \in \Omega,$$

for some $c > 0$. Dividing by ϵ implies

$$(A.15) \quad |\mu_0 \kappa(k - k_\star) + R_k| \geq c \kappa |k - k_\star|, \quad \forall \alpha_k \in \Omega,$$

with the same c . Using (3.2) with $n = 2$ gives

$$(A.16) \quad \begin{aligned} & \sum_{|k| \leq O(1/\epsilon)} \omega(x_0, \alpha_k) \varphi_1(\alpha_k) [\Delta\psi(H(x_0, \alpha_k, \epsilon); h) - \Delta\psi(a_k; h)] \\ &= \sum_{|k| \leq O(1/\epsilon)} \frac{O(\epsilon|k - k_*|^2)}{1 + |k - k_*|^{5/2}} = O(\epsilon^{1/2}). \end{aligned}$$

It is clear that all the big- O terms are uniform with respect to \tilde{x} (and, hence, h) restricted to a bounded set. Combining (A.7), (A.11), and (A.16) finishes the proof.

A.3. Proof of Lemma 3.2.

Denote

$$(A.17) \quad J := \int s^{-1} [\varphi'_3(s + q + \Delta q) - \varphi'_3(s + q)] ds,$$

where we omitted the dependence on α for simplicity. All the big- O terms in this subsection are uniform with respect to $\alpha \in \Omega$. By (3.13),

$$(A.18) \quad \varphi_3^{(l)}(p) = O(|p|^{(1/2)-l}), \quad p \rightarrow \infty, \quad l = 0, 1, 2.$$

Restricting the integral in (A.17) to $|s| \leq 1$ we find

$$(A.19) \quad J_1 := \int_{|s| \leq 1} s^{-1} [\varphi'_3(s + q + \Delta q) - \varphi'_3(q + \Delta q)] - [\varphi'_3(s + q) - \varphi'_3(q)] ds.$$

Clearly, $J_1 = O(|\Delta q|)$ uniformly in $|q| \leq c$. Here we have used (A.18) with $l = 3$. Using (A.18) with $l = 2$ with find also

$$(A.20) \quad J_2 := \int_{|s| \geq 1} s^{-1} [\varphi'_3(s + q + \Delta q) - \varphi'_3(s + q)] ds = O(|\Delta q|)$$

uniformly in $|q| \leq c$. Combining the estimates for $J_{1,2}$ proves the lemma.

A.4. Proof of Lemma 4.3.

Denote

$$(A.21) \quad A_n(\epsilon) := \epsilon \sum_k g^{(n)}(\epsilon(k - k_*)), \quad n = 0, 1, 2, \dots$$

For simplicity, the dependence of A_n on k_* is omitted from notation. All the estimates in this section are uniform with respect to k_* . Then

$$(A.22) \quad \begin{aligned} -A_0(\epsilon) &= \sum_k \int_{\epsilon(k - k_*)}^{\epsilon(k+1 - k_*)} (g(t) - g(\epsilon(k - k_*))) dt \\ &= \sum_k \sum_{j=1}^N \int_{\epsilon(k - k_*)}^{\epsilon(k+1 - k_*)} g^{(j)}(\epsilon(k - k_*)) \frac{(t - \epsilon(k - k_*))^j}{j!} dt + O(\epsilon^{N+1}) \\ &= - \sum_{j=1}^N \frac{\epsilon^j}{(j+1)!} A_j(\epsilon) + O(\epsilon^{N+1}). \end{aligned}$$

Arguing in the same way we get a more general statement:

$$(A.23) \quad A_M(\epsilon) = \sum_{j=1}^{N-M} \frac{\epsilon^j}{(j+1)!} A_{M+j}(\epsilon) + O(\epsilon^{N-M+1}), \quad M = 0, 1, \dots, N-1.$$

Clearly, $A_j(\epsilon) = O(\epsilon)$ for any $j = 0, 1, 2, \dots$. Applying (A.23) with $M = N-1, N-2, \dots, 0$ gives:

$$(A.24) \quad \begin{aligned} A_{N-1}(\epsilon) &= \epsilon O(|A_N|) + O(\epsilon^2) = O(\epsilon^2), \\ A_{N-2}(\epsilon) &= \epsilon O(|A_{N-1}|) + \epsilon^2 O(|A_N|) + O(\epsilon^3) = O(\epsilon^3), \dots, A_0 = O(\epsilon^{N+1}). \end{aligned}$$

Since $N > 0$ is arbitrary, the lemma is proven.

REFERENCES

- [1] C. L. Epstein, *Introduction to the mathematics of medical imaging*. Philadelphia: SIAM, second ed., 2008.
- [2] B. Li, G. B. Avinash, and J. Hsieh, “Resolution and noise trade-off analysis for volumetric CT,” *Medical Physics*, vol. 34, no. 10, pp. 3732–3738, 2007.
- [3] R. Grimmer, J. Krause, M. Karolczak, R. Lapp, and M. Kachelrie, “Assessment of spatial resolution in CT,” *IEEE Nuclear Science Symposium Conference Record*, pp. 5562–5566, 2008.
- [4] S. N. Friedman, G. S. Fung, J. H. Siewersden, and B. M. Tsui, “A simple approach to measure computed tomography (CT) modulation transfer function (MTF) and noise-power spectrum (NPS) using the American College of Radiology (ACR) accreditation phantom,” *Medical Physics*, vol. 40, no. 5, pp. 1–9, 2013.
- [5] H. Kruse, “Resolution of Reconstruction Methods in Computerized Tomography,” *SIAM Journal on Scientific and Statistical Computing*, vol. 10, pp. 447–474, 1989.
- [6] L. Desbat, “Efficient sampling on coarse grids in tomography,” *Inverse Problems*, vol. 9, pp. 251–269, 1993.
- [7] F. Natterer, “Sampling in Fan Beam Tomography,” *SIAM Journal on Applied Mathematics*, vol. 53, pp. 358–380, 1993.
- [8] F. Natterer, “Sampling and resolution in CT,” in *Proceedings of the Fourth International Symposium (CT-93): Novosibirsk, 1993* (M. M. Lavrentév, ed.), pp. 343–354, Utrecht: VSP, 1995.
- [9] V. P. Palamodov, “Localization of harmonic decomposition of the Radon transform,” *Inverse Problems*, vol. 11, pp. 1025–1030, 1995.
- [10] A. Caponnetto and M. Bertero, “Tomography with a finite set of projections: singular value decomposition and resolution,” *IEEE Transactions on Information Theory*, vol. 13, pp. 1191–1205, 1997.
- [11] A. Faridani and E. Ritman, “High-resolution computed tomography from efficient sampling,” *Inverse Problems*, vol. 16, pp. 635–650, 2000.
- [12] A. Faridani, “Sampling theory and parallel-beam tomography,” in *Sampling, wavelets, and tomography*, vol. 63 of *Applied and Numerical Harmonic Analysis*, pp. 225–254, Boston, MA: Birkhauser Boston, 2004.
- [13] A. Rieder and A. Schneek, “Optimality of the fully discrete filtered backprojection algorithm for tomographic inversion,” *Numerische Mathematik*, vol. 108, pp. 151–175, 2007.
- [14] S. H. Izen, “Sampling in Flat Detector Fan Beam Tomography,” *SIAM Journal on Applied Mathematics*, vol. 72, pp. 61–84, 2012.
- [15] P. Stefanov, “Semiclassical sampling and discretization of certain linear inverse problems,” *SIAM Journal of Mathematical Analysis*, vol. 52, pp. 5554–5597, 2020.
- [16] F. Monard and P. Stefanov, “Sampling the X-ray transform on simple surfaces,” *ArXiv ID:2110.05761*, 2021.
- [17] P. Stefanov, “The Radon transform with finitely many angles,” *arXiv:2208.05936v1*, pp. 1–30, 2022.
- [18] A. Katsevich, “A local approach to resolution analysis of image reconstruction in tomography,” *SIAM Journal on Applied Mathematics*, vol. 77, no. 5, pp. 1706–1732, 2017.
- [19] A. Katsevich, “Analysis of reconstruction from discrete Radon transform data in \mathbb{R}^3 when the function has jump discontinuities,” *SIAM Journal on Applied Mathematics*, vol. 79, pp. 1607–1626, 2019.
- [20] A. Katsevich, “Analysis of resolution of tomographic-type reconstruction from discrete data for a class of distributions,” *Inverse Problems*, vol. 36, no. 12, 2020.
- [21] A. Katsevich, “Resolution analysis of inverting the generalized Radon transform from discrete data in \mathbb{R}^3 ,” *SIAM Journal of Mathematical Analysis*, vol. 52, no. 4, pp. 3990–4021, 2020.
- [22] A. Katsevich, “Resolution analysis of inverting the generalized N -dimensional Radon transform in \mathbb{R}^n from discrete data,” *Journal of Fourier Analysis and Applications*, vol. 29, art. 6, 2023.
- [23] A. Katsevich, “Resolution of 2D reconstruction of functions with nonsmooth edges from discrete Radon transform data,” *SIAM Journal on Applied Mathematics*, vol. to appear, 2023.
- [24] A. Katsevich, “Novel resolution analysis for the Radon transform in \mathbb{R}^2 for functions with rough edges,” *arXiv:2206.04545*, pp. 1–32, 2022.
- [25] P. M. Joseph and R. A. Schulz, “View sampling requirements in fan beam computed tomography,” *Medical Physics*, vol. 7, no. 6, pp. 692–702, 1980.
- [26] G. Beylkin, “The inversion problem and applications of the generalized Radon transform,” 1984.

- [27] F. Natterer, *The Mathematics of Computerized Tomography*. Philadelphia: SIAM, 2001.
- [28] A. Katsevich, “An accurate approximate algorithm for motion compensation in two-dimensional tomography,” *Inverse Problems*, vol. 26, 2010.
- [29] A. G. Ramm and A. I. Zaslavsky, “Singularities of the Radon transform,” *Bull. Amer. Math. Soc.*, vol. 25, pp. 109–115, 1993.
- [30] A. G. Ramm and A. I. Zaslavsky, “Reconstructing singularities of a function given its Radon transform,” *Math. and Comput. Modelling*, vol. 18, no. 1, pp. 109–138, 1993.
- [31] F. D. Gakhov, *Boundary Value Problems*. Oxford: Pergamon Press, 1966.
- [32] A. P. Prudnikov, Y. A. Brychkov, and O. I. Marichev, *Integrals and series. Volume 1. Elementary functions*. New York: Gordon and Breach, 1986.
- [33] G. Nemes, “Error bounds for the asymptotic expansion of the Hurwitz zeta function,” *Proceedings of the Royal Society A: Mathematical, Physical and Engineering Sciences*, vol. 473, no. 2203, 2017.